IRE1α-XBP1 Activation Elicited by Viral Singled Stranded RNA via TLR8 May Modulate Lung Cytokine Induction in SARS-CoV-2 Pneumonia

José J. Fernández[1], Cristina Mancebo[1,2], Sonsoles Garcinuño[3], Gabriel March[3], Yolanda Alvarez[1,2], Sara Alonso[1], Luis Inglada[4], Jesús Blanco[5,6], Antonio Orduña[3], Olimpio Montero[1], Tito A. Sandoval[7,8,9], Juan R. Cubillos-Ruiz[7,8,9], Elena Bustamante[10], Nieves Fernández[1,2,¶], Mariano Sánchez Crespo[1¶*]

[1]Unidad de Excelencia Instituto de Biología y Genética Molecular, CSIC-Universidad de Valladolid, Spain

[2]Departamento de Bioquímica, Biología Molecular y Fisiología, Universidad de Valladolid, Spain

[3]Servicio de Microbiología, Hospital Clínico Universitario de Valladolid, Universidad de Valladolid, Spain

[4]Servicio de Medicina Interna, Hospital Universitario Rio-Hortega, Valladolid, Spain

[5]Servicio de Medicina Intensiva, Hospital Universitario Rio-Hortega, Valladolid, Spain

[6]CIBER de Enfermedades Respiratorias, Instituto de Salud Carlos III, Madrid, Spain

[7]Weill Cornell Graduate School of Medical Sciences, Cornell University, New York, NY, 10065, USA

[8]Department of Obstetrics and Gynecology, Weill Cornell Medicine, New York, NY, 10065, USA

[9]Sandra and Edward Meyer Cancer Center, Weill Cornell Medicine, New York, NY, 10065, USA

[10]Servicio de Medicina Intensiva, Hospital Clínico Universitario de Valladolid, Spain

* Corresponding author
E-mail: sanchezcrespomariano@gmail.com (M.S.C.)

[¶]These authors contributed equally to this work.

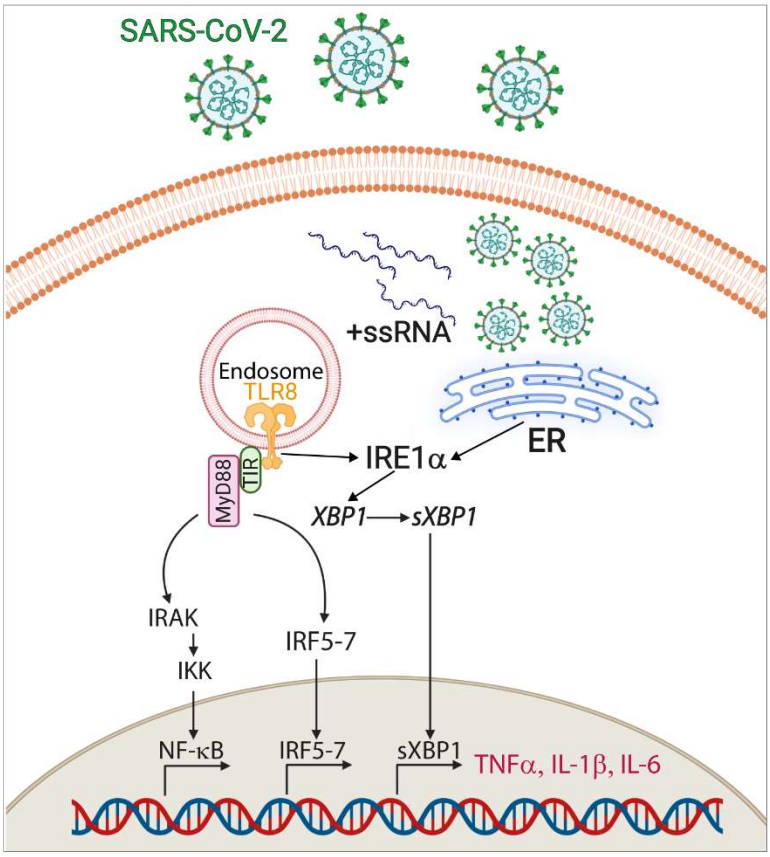

Abstract

Initial symptoms of COVID-19 infection depend on viral replication, while hyperinflammation is a hallmark of critical illness and may drive severe pneumonia and death. Among the mechanisms potentially involved in the hyperinflammatory state, we focused on the unfolded protein response, because the IRE1α-XBP1 branch can be activated as result of the endoplasmic reticulum stress produced by the overwhelming synthesis of viral components and synergizes with Toll-like receptor signaling to induce cytokine expression. Viral RNA may trigger the IRE1α-XBP1 branch via TLR7/8 activation and like TLR2 and TLR4 may underpin cytokine expression trough *XBP1* splicing (*sXBP1*). The expression of *IL1B*, *IL6*, and *TNF*

mRNA in bronchoalveolar aspirates (BAAs) were higher in COVID-19 patients under mechanical ventilation and intubation who showed *sXBP1*. The scrutiny of monocytic/macrophagic markers during active infection showed a reduction of those involved in antigen presentation and survival, as well as the IFN stimulated gene *MX1*. These changes reverted after infection tests turned negative. In contrast, the expression of the mRNA of the serine protease *TMPRSS2* involved in S protein priming showed a high expression during active infection. *TLR8* mRNA showed an overwhelming expression as compared to *TLR7* mRNA, which suggests the presence of monocyte-derived dendritic cells (MDDCs). *In vitro* experiments in MDDCs activated with ssRNA40, a positive-sense, single-stranded RNA (+ssRNA) like SARS-CoV-2 RNA, induced *sXBP1* and the expression of IL-1β, IL-6, and TNFα at mRNA and protein levels. These responses were blunted by the IRE1α ribonuclease inhibitor MKC8866. Given the analogies between the results observed in BAAs and the effects induced by +ssRNA in MDDCs, IRE1α ribonuclease inhibition might be a druggable target in severe COVID-19 disease.

Author summary

COVID-19 pandemics put an unprecedented pressure on health systems. The need of new therapies urged research on the mechanisms triggered by the interaction of SARS-CoV-2 virus with host cells and the ensuing pathophysiology driving pneumonia and multiorgan failure. Hyperinflammation soon appeared as a mechanism involved in mortality that could even proceed after viral infection comes to an end. Hyperinflammation is supported by an inappropriate production of cytokines, and this explains the use of the term cytokine storm to refer to this phase of the disease.

Given that insight into the molecular mechanisms driving cytokine storm should focus on the interaction of viral components with immune cells, experiments addressing the effect of viral components on its cognate receptors were carried out. It was observed that viral RNA induces a cytokine pattern like the one observed in bronchoalveolar aspirates of COVID-19 patients with critical disease. Overall, the study revealed that both cell organelle overload and receptors involved in the recognition of viral RNA may team up to induce proinflammatory cytokines. This mechanism can be exploited to develop new treatments for COVID-19 disease.

Introduction

Coronavirus disease 2019 (COVID-19) is a pandemic infection produced by severe acute respiratory syndrome coronavirus 2 (SARS-CoV-2). Habitual evolution includes an initial influenza-like phase where fever and unproductive cough are predominant, but it can lead to severe respiratory insufficiency and multiorgan failure, which in many cases proceeds after infection resolution due to a hyperinflammatory response associated with the production of proinflammatory cytokines. The term cytokine storm was coined to refer to this condition [1], but the analysis of the immunopathological damage and the analogies with other viral diseases make it most appropriate the use of viral sepsis to depict the association of T-cell deficiencies with systemic hyperinflammation driven by virus-host cell interaction [2]. The use by viruses of the translational machinery of the host to produce their materials overloads many cellular functions, including protein folding and secretion in the endoplasmic reticulum (ER). Since only properly folded proteins should exit from the ER to maintain homeostasis, cells arrange a response directed to retain and degrade defective proteins. This involves an intracellular signaling pathway termed the unfolded protein response (UPR) [3-5]. The UPR includes a down regulation of global protein synthesis, the degradation of some proteins, and the transcriptional induction of specific genes associated with the activity of its three branches. The most conserved one depends on the dual activity of inositol-requiring enzyme 1α (IRE1α), which shows protein kinase and endonuclease activities [6]. The endonuclease activity cleaves a 26- base fragment of the mRNA of the preformed transcript of *XBP1*, which is followed by ligation of the resulting exons to yield *sXBP1*. This drives the translation of the functionally active factor sXBP1 that *trans*-activates genes encoding proinflammatory proteins, e.g., the prostaglandin producing enzymes cyclooxygenase 2 and the microsomal isoform of

prostaglandin synthase 2 [7], the ubiquitin-like modifier ISG15, and the cytokines IFNβ, IL-6, IL-23, and TNFα [8-11].

Although the goal of the UPR is alleviating ER-stress, the IRE1α-XBP1 branch contributes to the pathogenesis of multiple ailments, including cancer, atherosclerosis, infections, and autoimmune diseases [12-15]. Recent research has disclosed that the IRE1α-XBP1 branch enhances viral transcription and contributes to maintain dormant viral genomes in a host of infections [16,17]. The notion that UPR branches can mediate immune recognition of zoonotic viruses and drive acute lung injury through ER-stress mediated inflammation was disclosed by Hrincius et al. [18], who showed activation of the UPR by infection with poorly glycosylated pandemic strains of influenza A virus. The IRE1α route was recruited, and its activation reduced when glycans were added to specific sites in the globular head of hemagglutinin. A study in cell lines infected with a SARS-CoV-2 isolate and lung biopsies of COVID-19 patients showed that SARS-CoV-2 hijacks the glycosylation biosynthetic machinery and drives ER-stress and UPR activation. This is due to the overwhelming asparagine N-linked glycosylation required for the translation of viral glycoproteins, which forces aberrant glycosylation and ER-stress [19]. In keeping with notion, specific activation of sXBP1 has been reported in monocytes from COVID-19 patients [20].

The association of sXBP1 with TLR2 and TLR4 signaling [8] together with genuine UPR induced by protein synthesis overload point to sXBP1 involvement in the cytokine storm. [21]. The role of cytokine storm in COVID-19 disease was supported by the beneficial effect of tocilizumab, a humanized antihuman IL-6 receptor antibody [22]. This is noteworthy given the dependence of IL-6 production on the IRE1α-XBP1 branch [8] and the presence in the proximal promoter of *IL6* of at least six sequences binding to sXBP1 [23]. Another potential interference of sXBP1 on COVID-19 illness stems from its blunting effect on dendritic cell homeostasis and the metabolic fitness of T-cells [24,25]. Likewise, the σ1 receptor (S1R)

reduces cytokine production in murine models of septic shock through IRE1α endonuclease activity inhibition [14]. A new piece of evidence associating the UPR with COVID-19 illness was the induction of the UPR by ORF8 and S viral proteins, as well as the reduction of viral replication by pharmacological inhibition of the IRE1α and ATF6 branches in epithelial cell lines [26]. In contrast, up-regulation of IRE1α (RNase) activity by cannabidiol has been found to block SARS-CoV-2 replication in a cell line derived from lung epithelial cells and in lungs and nasal turbinates of infected mice [27].

Given that SARS-CoV-2 is a +ssRNA virus, the tandem TLR7/8 comes into prominence given its ability to bind viral RNA. Consistent with this notion, loss-of-function variants in X-chromosomal *TLR7* have been reported in young patients with severe COVID-19 disease, who showed impaired type I and II IFN responses [28]. The purpose of this study has been addressing how sXBP1 and TLR7/8 engagement may underpin viral sepsis in COVID-19 disease. To this end, samples of nasopharyngeal swabs and bronchoalveolar aspirates (BAAs) were studied to address the presence of *sXBP1*, the cytokine-signature, and the expression of monocytic lineage cell markers and enzymes involved in energetic metabolism. After obtaining a profile of the transcriptional landscape, *in vitro* experiments were performed to address the transcriptional and energetic patterns of MDDCs stimulated with TLR7 and TLR8 agonists. Experiments showed that TLR8 activation of MDDCs induces a pattern of *XBP1* splicing and cytokine expression, sensitive to inhibition of IRE1α RNase activity, which mimics the pattern observed in BAAs.

Results

Studies in Nasopharyngeal Samples

Initial assays were conducted in nasopharyngeal samples from patients receiving medical assistance for symptoms consistent with COVID-19 disease (Fig 1A). The extracted RNA was used for the diagnosis of SARS-CoV-2 infection and residual samples used for the assay of *sXBP1* by RT-PCR assays. This entails the separation of the PCR products by electrophoresis in agarose gel and densitometric analysis of GelRed stained bands. *sXBP1* is distinguished from unspliced *XBP1* (*uXBP1*) by its faster migration. The position of the primers and the spliced region are shown in Fig 1B. These correspond to GenBank sequence NM_001079539.2, which differs from *uXBP1* sequence NM_005080.4 by the deletion of 26 nucleotides. Separate sequencing of the bands was used to confirm splicing (Fig 1C). A random selected array of RT-PCR negative and positive samples shows the presence of *uXBP1* and *sXBP1* (Fig 1D). The presence of three bands in some cases is explained by the formation of heteroduplexes [29]. *sXBP1* was detected in 17.91% of SARS-CoV-2 negative and 40.32% of SARS-CoV-2 positive patients (Fig 1E). Quantitation of *sXBP1* showed higher values in COVID-19 positive patients as compared to the negative ones (Fig 1F). The incidence of *sXBP1* was similar in male and females (Fig 1G) and increased with age (Fig 1H). Mortality was observed in four patients who showed a degree of splicing above 10% of total *XBP1* (Fig 1I). These findings show that *sXBP1* shows higher frequency and extent in nasopharyngeal exudates of patients with active SARS-CoV-2 infection, particularly in dying patients.

sXBP1 and Cytokine Expression in BAAs

Further experiments were carried out using RNA extracted from BAAs of patients under mechanical ventilation in intensive care unit (ICU) (Fig. 2A). Ventilatory support and

endotracheal intubation were indicated because of acute hypoxemic respiratory failure despite high-flow nasal oxygen therapy or non-invasive ventilation. COVID-19 patients received a standard and proved useful treatment for the hyperinflammatory state consisting of 6 mg dexamethasone daily or 50 mg of IV hydrocortisone every 8 hours for up to 10 days, while this protocol was not routinely used in non-COVID-19 patients (Fig 2B). The extent of *sXBP1* was higher in SARS2-CoV-2 pneumonia patients than in those with respiratory failure due to other conditions, decreased after COVID-19 tests turned negative, and showed higher values than those observed in nasopharyngeal swabs (Fig 2C). The PERK-eIF2α-ATF4-CHOP branch of the UPR was explored assaying *DDIT3*/CHOP gene expression. *DDIT3* expression also decreased after SARS-CoV-2 tests turned negative, while there was no significant difference of expression between non-COVID-19 and COVID-19 pneumonia patients (Fig 2D). As regards cytokine expression (Fig 2E-2N), *IL1B* and *IL6* mRNA levels during viral proliferation were significantly lower than those detected in non-COVID-19 patients. A similar trend was observed in *TNF*, *IL23A*, and *IL8* mRNA expression, although these values did not reach statistical significance. Cytokine mRNA did not show a trend to decrease after SARS-CoV-2 tests were negative. *IL10* and *IFNB* mRNA were higher in SARS-CoV-2 infection than in non-COVID pneumonia and continued elevated after COVID-19 tests turned negative. *IFNG* showed a trend to be increased in COVID-19 pneumonia. Overall, these results show that *sXBP1* in respiratory samples from COVID-19 patients does not associate with levels of cytokine expression higher than those observed in non-COVID-19 pneumonias. The high expression of *IL10* mRNA suggests a parallel activation of an archetypal anti-inflammatory cytokine that might counter the inflammatory response. The increased expression of *IFNB1* mRNA is consistent with its involvement in viral sepsis.

***sXBP1* Stratification in SARS-CoV-2 Patients during ICU Hospitalization**

SARS-CoV-2 patients were stratified according to the presence or absence of both active infection and *sXBP1*. Fig 3A shows viral load in samples collected during infection and at the time when a negative COVID-19 test was first recorded. *PTGS2* mRNA was higher in patients with *sXBP1* both during infection and after negativization of the RT-PCR test (Fig 3B). *TNF* and *IL1B* mRNA expression was also higher in patients with *sXBP1*, even after a negative RT-PCR test (Fig 3C and 3D). *IL6* mRNA was increased in patients with *sXBP1* and active infection (Fig 3E). *IL8* mRNA was expressed at much lower levels than those encoding other cytokines, particularly after negativization of the infection in patients who did not show *sXBP1* (Fig 3F). *IL10* mRNA was higher in SARS-CoV-2 positive patients who did not show *sXBP1* and remained elevated in patients showing *sXBP1* after resolution of the infection. These results show a high expression of the mRNA of *PTGS2* and several proinflammatory cytokines in patients with *sXBP1*, which may persist after SARS-CoV-2 test becomes negative. The sustained expression of *PTGS2* (COX2) mRNA suggests its involvement in either induction or repair of inflammatory damage [30]. Together, the results agree with the reported role of sXBP1 in the transcriptional activation of COX2, TNFα, IL-1β, and IL-6.

Expression of Genes Involved in Glycolysis and Oxidative Phosphorylation (OXPHOS)

Lymphocytes and myeloid cells respond to pathogen-associated molecular patterns (PAMPs) with a robust rewiring of their energetic metabolism driving increased glycolysis (Fig 4A). The impairment of O_2 supply due to pneumonia further explains the resort to glycolysis and agrees with reports showing that SARS-CoV-2-induced metabolic reprogramming enhances the production of proinflammatory cytokines and IFNs by monocytes, and concomitantly inhibits T cell function [31,32]. Consistent with this notion, the expression of *GLUT1* mRNA, a glucose transporter, and *HIF1A* mRNA, a transcription factor involved in the regulation of glycolytic enzymes, were increased during active infection. However, there was no difference as

compared to non-COVID-19 pneumonia (Fig 4B and 4C). The mRNA encoding hexokinase II (Fig 4D), pyruvate dehydrogenase kinase IV (Fig 4F), malate dehydrogenase (MD) 2 (Fig 4G), and *cis*-aconitate dehydrogenase (*IRG1* gene) (Fig 4K) increased during active infection as compared to both non-COVID-19 pneumonia and post-COVID infection. Notably, proteins involved in mitochondrial function also increased during COVID-19 pneumonia, i.e., succinate dehydrogenase subunit A (Fig 4I) and the 2-oxoglutarate-malate transporter SLC25A11, (Fig 4J). Together, these data show a resort to glycolysis during active SARS-CoV-2 infection that seems supported by the activity of HIF1and elements of the malate-aspartate shuttle such as MD2 and SLC25A11, which buttress the NAD^+/NADH redox balance necessary for the progression of glycolysis at the glyceraldehyde 3-phosphate-dehydrogenase step.

Characterization of Monocytic Markers in BAAs

The first attempt to characterize the monocytic/macrophagic populations in BAAs focused on the expression of TLR7/8, given their involvement in the recognition of viral RNA. *TLR8* mRNA was expressed to a far greater extent than *TLR7* mRNA (Fig 5A), which agrees with the decay of *TLR7* expression during the differentiation to MDDCs [33]. Further assay of markers showed a diminished expression of *HLA-DRB1* (Fig 5B), a gene involved in antigen presentation, *CD300E* (Fig 5C), a gene associated with survival signals, the chemokine receptor *CCR2* (Fig 5D), and the IFN-stimulated gene (ISG) *MX1*, (Fig 5G). Negativization of viral replication was associated with an increase of the expression of these genes, as well as the migration receptor *MMP9* (Fig 5E) and the MDDC differentiation marker *BATF3* (Fig 5F). *PTGS2*/COX2 mRNA was similar in non-COVID and active COVID infection and decreased after RT-PCR test became negative (Fig 5I). The mRNA of the ISG *OAS1* did not show significant changes during SARS-CoV-2 infection and increased after negativization of SARS-CoV-2 test (Fig 5H). *TMPRSS2* mRNA, a serine protease involved in the cleavage of viral

spike proteins [34] was significantly increased during SARS-CoV-2 active infection and (Fig 5J). These results disclose a differentiation profile during COVID-19 infection characterized by a low expression of markers associated with antigen presentation and survival signals, as well as *MX1*. This is followed by an increase of the markers expressed in MDDCs in response to TLR ligands [33]. The high expression of *TMPRSS2* mRNA underscores the role of TMPRSS2 in SARS-CoV-2 cell invasion and the low expression of *MX1* agrees with the reported association of single nucleotide polymorphisms within *TMPRSS2* and near *MX1* gene with severe COVID-19 disease [35]. A cogent explanation for the low *MX1* expression could be an evasive strategy of SARS-CoV-2 to avoid and/or shut down type I IFN responses [36].

Effects Induced by the Stimulation of Receptors Involved in the Recognition of Viral RNAs in MDDCs

Because SARS-CoV-2 is a +ssRNA virus, we posited that TLR7/8 might shape the innate immune response, given their endosomal location and accessibility to intracellular viral RNA. *TLR7* and *TLR8* expression in MDDCs mimicked the pattern observed in BAAs by showing a high expression of *TLR8* and a low expression of *TLR7* mRNA (Fig 6A). Activation of TLR7 by the selective ligand imiquimod showed a low extent of *XBP1* splicing, even in real-time RT-PCR assays using a reverse primer overlaping the spliced region (Fig 6B). Consistent with the effect of palmitate as a potentiator of imiquimod effect via metabolic rewiring and *XBP1* splicing [11], the expression of proinflammatory cytokines increased in the presence of palmitate (Fig 6C-6F). In contrast, 2-deoxyglucose, which enhances *XBP1* splicing in the presence of some PAMPs [10] showed a limited effect. Given that IFNγ teams up with TNFα to induce mortality in mice during SARS-CoV-2 infection [37] and it has been associated with the development of cytokine storm [38-41], the expression of ISGs was assayed. In contrast to IFNs, *MX1* and *OAS1* showed high levels of expression. The IRE1α RNase inhibitor MKC8866

[42] and the S1R agonist fluvoxamine, which has been reported to inhibit *XBP1* splicing in bacterial sepsis [14], lacked any significant effect on those responses (Fig 6G-6J). Real-time assays of energetic metabolism with the Seahorse technology, showed a reduction of O_2 consumption rate (OCR) and an increased extracellular acidification rate (ECAR) in response to imiquimod (Fig 6K), thus mimicking the glycolytic rewiring induced by bacterial PAMPs [43]. These effects were enhanced by metformin, a well-known inhibitor of the complex I of the electron transport chain (Fig 6L) that has been associated with a beneficial effect on the evolution of COVID-19 disease [44], most likely explained by its ability to reduce IL-1β and enhance IL-10 production [45]. Poly(cytidylic-inosinic) acid (poly(I:C)), a polyribonucleotide that mimics the effects of viral double-stranded RNA and activates TLR3, did not show any significant effect (Fig 6M).

In contrast to the limited effect of imiquimod, the TLR8 agonist ssRNA40, a 20-mer phosphorothioate protected single-stranded RNA oligonucleotide containing a GU-rich sequence, induced *sXBP1* in a similar way to the effect of the TLR2 agonist zymosan. The splicing was blocked by the IRE1α RNase inhibitors MKC8866 and 4μ8C (Fig 7A). MKC8866 also inhibited the expression of *IL1B*, *IL6*, and *TNF* mRNA (Figs 7B-7D) and protein (Fig 7E-7F), thus resembling the cytokine signature detected in BAAs. ssRNA41, a ssRNA40 derivative wherein uracil nucleotides are replaced with adenosine and does not activate TLR8-dependent signaling, did not induce cytokine expression, induced *sXBP1* to a low extent, and was less active than ssRNA40 to induce the aggregation of misfolded proteins, as deemed from the assay of aggresomes (S1A and S1B Fig). While pro-IL-1β expression increased in response to ssRNA40 (Fig 7G), IL-1β was not detected in MDDCs supernatants, thus suggesting that ssRNA40 does not activate the inflammasome and that an additional signal(s) is required for IL-1β secretion. The expression of IL-6 and TNFα protein was inhibited by both MKC8866 and fluvoxamine, which suggests that sXBP1 plays a significant role on the transcription of

these cytokines. *IFNB1*, *MX1*, and *OAS1* mRNA were also induced by ssRNA40, while both MKC8866 and fluvoxamine only inhibited *MX1* and *OAS1* expression (Fig 7H-7K), thus suggesting a direct effect of sXBP1 on *MX1* and *OAS1* expression, rather than an indirect effect mediated by IFNs. Notably, ssRNA40 did not modify the energetic pattern of MDDCs (S1C Fig), which indicates that its ability to induce cytokine expression does not depend on blatant energetic changes. Unlike ssRNA40, zymosan, a ligand of TLR2 and C-type lectin receptors that mimics the external wall of fungi, induced a robust induction of glycolysis and OXPHOS as deemed from ECAR and OCR increases, respectively (S1D Fig).

To confirm the involvement of sXBP1 in the transcriptional activation of cytokines, its binding to the proximal promoter regions of *IL1B*, *IL6*, and *TNF* was assayed. Chromatin immunoprecipitation (ChIP) assays were conducted with primers spanning areas including consensus *cis*-regulatory elements associated with position weight matrices discovered in sXBP1 target promoters [23]. An increased binding of sXBP1 to the regions indicated in Fig 7L-N was observed after one hour of stimulation by ssRNA40. These results show that PAMPs acting on TLR8 induce a cytokine signature like that observed in BAAs and point to the central involvement of MDDCs in the innate immune response to SARS-CoV-2. The presence of *sXBP1* in nasopharyngeal swabs and BAAs, its induction by ssRNA40 in MDDCs, the effect of IRE1α RNase inhibition on the cytokine induction produced by ssRNA40, and the demonstration of sXBP1 binding to the *IL1B*, *IL6*, and *TNF* promoters suggest that TLR8-induced *XBP1* splicing may contribute to the viral sepsis observed in severe cases of COVID-19 disease.

Discussion

Current pathogenetic views on COVID-19 pneumonia focus on immunopathological damage due to an exuberant innate immune response and a poor adaptive response. Assay of respiratory secretions allows the identification of the pathogens and can also give cues on pathogenesis [46-48]. This approach has been used in COVID-19 disease after the seminal studies by Zhou et al. [49] and Liao et al. [50], who used bronchoscopy and lavage to identify immune cell types in the respiratory tract. Our study focussed on patients under mechanical ventilatory support due to severe pneumonia, whose samples were obtained during routine care by attending staff [51-53]. This is in line with the use of tracheal aspirates to assess the transcriptional profiling of the lower respiratory tract in critically ill COVID-19 patients [54]. Initial assays showed higher degrees of *sXBP1* in COVID-19 disease than in patients with non-SARS-CoV-2 infection, although the mRNA levels of proinflammatory cytokines were higher in patients undergoing bacterial pneumonia. This was not fully unexpected, since cytokine storm is influenced by genetics and physiological conditions, in addition to cytokine levels [55,56]. Moreover, COVID-19 patients received steroids in a regular schedule, which contributes to reduce proinflammatory cytokines, and showed an overall mortality lower than that observed in non-COVID patients. Notably, inhibition of IRE1α activity through activation of S1R by fluvoxamine protected mice from mortality during endotoxemia and fecal-induced peritonitis, as well as the production of IL-1β, IL-6, and IL-12 p40 by human leukocytes [14]. Consistent with the experimental results, early fluvoxamine treatment in individuals with mild COVID-19 illness was associated with a reduction of signs of clinical deterioration as compared to the placebo group [57]. Similar results were reported in the TOGETHER trial, which involved larger cohorts for study and showed a significant reduction of morbidity by fluvoxamine, as deemed from a reduced resort to either retention in a COVID-19 emergency

setting or transfer to tertiary hospital. Consistent with these findings, an independent data safety monitoring committee recommended stopping randomly assigning patients to the fluvoxamine arm in view of the superiority criterion for the primary endpoint [58]. Stratification of patients showing active infection and *sXBP1* disclosed the association of *sXBP1* with higher levels of cytokine expression and their decrease after infection negativization, thus suggesting that the effect of fluvoxamine may be due to inhibition of the IRE1α-XBP1 branch.

Secondary goals of the study were the characterization of enzymes involved in the bioenergetics and the identification of myeloid-lineage differentiation footprints. Bioenergetic screening suggested active glycolysis during SARS-CoV-2 infection supported by HIF1 and elements of the malate-aspartate shuttle. However, the predominance of glycolytic enzymes cannot be straightforwardly construed as a proof of aerobic glycolysis or Warburg effect given the compromise of O_2 supply associated with SARS-CoV-2 pneumonia. The strong induction of *IRG1*/ACOD1 mRNA is consistent with its dependence on IFNs [59,60]. Notably, the ACOD1 product itaconate exerts antiviral activity and is considered a druggable target to counter the hyperinflammatory response [61].

Monocytic lineage cells are key players of the innate immune response due to their array of pattern recognition receptors and involvement in antigen presentation. BAAs showed a low expression of markers associated with antigen presentation, survival signals, and the ISG *MX1* during active infection. It is remarkable the low expression of *HLA-DRB1* mRNA, the gene encoding the most prevalent β-subunit of HLA-DR. This is in accordance with the decreased expression of HLA-DR in monocytes of COVID-19 patients, which drives hyperinflammation and defective antigen presentation mediated by IL-6 [62]. In contrast, the increased expression of *TMPRSS2* mRNA agrees with the facilitating role of this transmembrane protease in viral infection by cleaving viral S glycoprotein. Tellingly, single

409 nucleotide polymorphisms at 21q22.3 locus within *TMPRSS2* and near *MX1* genes have been
410 associated with severe COVID-19 disease [35].

411 TLR7 and TLR8 are tandem duplicated genes on the X-chromosome, the function of
412 which shows some commonalities and specificities. For instance, TLR8 is not functional in
413 mice, and this explains the involvement of TLR7-induced cytokines in murine influenza [63].
414 TLR8 expression is a hallmark of human MDDCs, while TLR7 is present in monocytes,
415 macrophages, and plasmacytoid dendritic cells [33]. A pioneering study addressing the
416 pathophysiology of 2003 SARS-CoV-1 outbreak showed a unique ability of SARS-CoV-1 GU-
417 rich RNA sequences to induce proinflammatory cytokines through TLR7 in mice and TLR8 in
418 human leukocytes [64]. This notion was extended in a recent report by comparing the effect of
419 GU-rich RNAs on inflammasome activation and proinflammatory cytokine production.
420 Notably, GU-rich RNA from the SARS-CoV-2 spike protein triggered the greatest
421 inflammatory in human macrophages via TLR8 [65]. This agrees with our BAA and *in vitro*
422 studies showing TLR8 as a central element in the recognition of +ssRNA virus and suggests a
423 unique involvement of MDDCs and TLR8 in *XBP1*splicing and hyperinflammation.
424 Comparison of ssRNA40 and ssRNA41 effects show that TLR8-dependent signaling and
425 sXBP1 are critical for cytokine expression, given the lack of effect of ssRNA41.

426 Activation of TLR7 by imiquimod induced a limited set of MDDC responses. However,
427 it was remarkable the effect on energetic metabolism, characterized by a drop of the OCR and
428 a parallel increase of ECAR, which mimicked the well-known effect of bacterial
429 lipopolysaccharide. The effect on cytokines and *sXBP1* was negligible and only reached
430 significant values in the presence of palmitate. Unfortunately, our study does not contribute to
431 answer open questions regarding the actual role of TLR7 in SARS-CoV-2 defense and
432 immunopathology. TLR7 mutations driving loss-of-function in the antiviral response have
433 been associated with severe forms of COVID-19 disease in young male [28]. Another study

showed that while some TLR7 variants exhibit a robust loss-of-function on type I IFNs production, other variants only have a marginal effect, thus suggesting that TLR7 may shape the anti-viral response through additional mechanisms [66]. Moreover, autosomic inborn errors of TLR3- and IRF7-dependent type I IFN immunity were found in 23 out of 659 patients with severe COVID-19 pneumonia [67], thus stressing the role of type I IFNs in the protection against severe forms of COVID-19 pneumonia. Our data agree with Ito et al. [68] findings, who first disclosed that the TLR7/TLR8 agonist R848 was 100-fold as potent as imiquimod in human MDDCs. The absence of energetic rewiring induced by ssRNA40 could be explained by IFNβ effect, since IFNβ restrains aerobic glycolysis during mycobacteria infection. This drives mitochondrial stress and helps explain why type I IFN may cause damaging effects to the host [69]. Consistent with this interpretation is the lack of effect of poly(I:C), a selective activator of TLR3 that by using TRIF as the sole adaptor, activates IRF3 and ultimately induces type I IFNs. This is in shark contrast with the effect of zymosan, a ligand for TLR2 and the C-type lectin receptor dectin-1 [70]. The binding of sXBP1 to *IL1B*, *IL6*, and *TNF* promoters induced by ssRNA40, together with the strong reduction of cytokine expression by an inhibitor of IRE1α RNase, further indicates that the IRE1α-XBP1 branch underpins the production of cytokines via TLR8. These results assign to TLR8 capacities previously reported for TLR2 and TLR4, where sXBP1 is required for sustained production of proinflammatory cytokines. A corollary to these results is that inhibition of IRE1α RNase activity could be a therapeutic approach for severe COVID-19 disease.

Materials and Methods

Patients, Leukocyte Samples, and Ethic Statements

Nasopharyngeal samples were obtained from patients studied in different medical departments for symptoms consistent with SARS-CoV-2 infection at *Hospital Clínico Universitario de Valladolid*. In the case of patients with mechanical ventilation and intubation, samples were obtained by endotracheal aspirations to remove respiratory secretions as part of clinical care by the attending staff. This allows the obtention of material from the alveolar and respiratory bronchiole level. BAAs were directly transferred to the DNA/RNA extraction kit MagMAX™ Pathogen RNA/DNA (Applied Biosystems) for the automated extraction machine Kingfisher Flex (Thermo Fisher Scientific). Infection diagnosis was obtained using a TaqPath™ COVID-19 RT-PCR kit assay from Applied Biosystems that targets N, ORF1a, and S genes. Resolution of infection was confirmed by the analysis of samples collected four days after a positive test. BAAs from non-COVID-19-patients were obtained from samples collected for microbiological diagnosis in patients suffering from severe bacterial pneumonia and requiring ventilatory support and intubation at ICU. Lung protective ventilation of both COVID-19 and non-COVID-19 patients was performed according to the current guidelines on mechanical ventilation of acute respiratory distress syndrome in adult patients, which makes it unlike the induction of cytokine expression by mechanical ventilation [71]. The clinical part of the study was approved by the Ethics Committee of *Area de Salud Valladolid Este* (ref. PI-GR-20-2011 COVID). For *in vitro* experiments, MDDCs were obtained from human mononuclear cells collected from pooled buffy coats of healthy donors provided by *Centro de Hemoterapia y Hemodonación de Castilla y León Biobank*. The study was approved by the Bioethical Committee of the Spanish Council of Research (CSIC) and the written informed consent of all healthy donors was obtained at *Centro de Hemoterapia y Hemodonación de Castilla y León*

Biobank. The researchers received the samples in an anonymous way. The process is documented by the Biobank authority according to the specific Spanish regulations. The ethics committee approved this procedure before starting the study. The differentiation of monocytes was carried out in the presence of GM-CSF and IL-4 for 5 days. Culture was carried out in RPMI 1640 medium containing 11.1 mM D-glucose and 4 mM L-glutamine. 10% FBS was maintained during the differentiation process and reduced to 2% at the start of experiments. Imiquimod (Sigma-Aldrich), ssRNA40/LyoVec™, and its negative control ssRNA41/LyoVec™ (InvivoGen) were used as TLR7 and TLR8 selective ligands in MDDCs. MKC8866 was from MedChemExpress.

XBP1 Splicing Assay

This was carried out by RT-PCRs using primers outside the spliced region. The PCR conditions were 5 min at 95°C (hot start), 45 cycles of denaturation at 95°C for 15 s, annealing at 60°C for 20 s and elongation at 72°C for 1 min. Final extension was carried out at 72°C for 5 min. Gel electrophoresis was carried out in 3% agarose and *sXBP1* and *uXBP1* bands were visualized by GelRed® staining and quantified using GelDoc Go Image System (Bio-Rad).

Real-Time RT-PCR and Protein Assays

Total RNA obtained by automatic extraction was used for RT reactions. The resulting cDNA was amplified in a LightCycler® 480 equipment using SYBR Green I mix containing Hot Start polymerase. Cycling conditions were adapted to each set of primers. *ACTB* was used as a housekeeping gene to assess the relative abundance of the different mRNA using the comparative cycle threshold method. The procedure was used to assay *XBP1, DDIT3, IL1B*, *IL6*, *IL10*, *IL23A*, *TNF*, *SLC25A11*, *GLUT1*, *HK2, PFKB3*, *PDK4*, *IDH1, IDH2, SDHA*, *MDH2*, *HIF1A*, *TLR7*, *TLR8*, *HLA-DRB1*, *CD300E*, *CCR2*, *MMP9*, *BATF3*, *MX1*, *OAS1*,

PTGS2, and *TMPRSS2* mRNA. Primer sequences are shown in Table 1. IL-6 and TNFα proteins were assayed in supernatants of MDDCs stimulated with ssRNA40 using kits from Elabscience. Pro-IL-1B was assayed by Western blot using an antibody from Cell Signaling Technology.

Table 1. Sequences of primers used for qRT-PCR and ChIP assays

GENE	Forward primer	Reverse primer
XBP1	5'- TGAGCTGGAACAGCAAGTGG -3'	5'- ATACCGCCAGAATCCATGGGGA -3'
sXBP1	5'- TGAGCTGGAACAGCAAGTGC -3'	5'- CTGCACCTGCTGCGGACTCA -3'
DDIT3	5'- GCAGAGATGGCAGCTGAGTC -3'	5'- AGCCAAGCCAGAGAAGCAGGGT -3'
IL1B	5'- ATGATGGCTTATTACAGTGGCAA -3'	5'- GTCGGAGATTCGTAGCTGGA -3'
TNF	5`-GTTGTAGCAAACCCTCAAGC-3´	5`-TTGAAGAGGACCTGGGAGTA-3´
IL6	5'- TTCGGTACATCCTCGACGGC -3'	5'- TCTGCCAGTGCCTCTTTGCT -3'
IL8	5'- ATTTCTGCAGCTCTGTGTGAA -3'	5'- AACTTCTCCCGACTCTTAAGT -3'
IL10	5´-GAGAACAGCTGCACC CAC TT-3´	5´-GGCCTTGCTCTTGTT TTCAC-3´
IL23A	5`- GTTCCCCATATCCAGTGTGG -3'	5'- TTAGGGACTCAGGGTTGCTG -3'
IL12B	5'- CATGGGCCTTCATGCTATTT -3'	5'- TTTGCATTGTCAGGTTTCCA -3'
IFNB1	5'- TCTAGCACTGGCTGGAATGAG- 3'	5'- GTTTCGGAGGTAACCTGTAAG-3'
IFNG	5'-CCAACGCAAAGCAATACATGA-3'	5'-CCTTTTTCGCTTCCCTGTTTTA-3'
N Gene	5'- CAATGCTGCAATCGTGCTAC -3'	5'- GTTGCGACTACGTGATGAGG -3'
COX2	5'- TTCAAATGAGATTGTGGGAA -3'	5'- AGATCATCTCTGCCTGAGTA -3'
GLUT1	5'- GAAGAGAGTCGGCAGATGAT- 3'	5'- AATAGAAGACAGCGTTGATGC -3'
HIF1A	5´-AGTGTACCCTAACTAGCCGA-3´	5´-GTGCAGTGCAATACCTTCC-3´
HK2	5'- TAGGGCTTGAGAGCACCTGT -3'	5'- CCACACCCACTGTCACTTTG -3'
PFKFB3	5'-CCGTTGGAACTGACGCAGA -3'	5'-CACAGGATCTGGGCAACGAG-3'
PDK4	5'- CCCGCTGTCCATGAAGCAGC -3'	5'-CCAATGTGGCTTGGGTTTCC-3'
MDH2	5'- TCGGCCCAGAACAATGCTAAA -3'	5'- GCGGCTTTGGTCTCGATGT -3'
IDH2	5'- TGGCTCAGGTCCTCAAGTCT -3'	5'- CTCAGCCTCAATCGTCTTCC -3'
SDHA	5'- CAGCATGTGTTACCAAGCT -3'	5' -GGTGTCGTAGAAATGCCAC -3'
SLC25A11	5'- ACACCGTCCTCACCTTCATC -3'	5'- CAGGGGGTAGAACAGACCAA -3'
IRG1	5'- GTTCCTGGGAACCACTACG -3'	5'- GATGTCTGGCTGACCCCAA -3'
TLR7	5´-CTTGGCACCTCTCATGCTCT-3'	5`-GTCTGTGCAGTCCACGATCA-3'
TLR8	5' -GCTGACCTGCATTTTCCTGC-3`	5`-CCGTTTGGGGAACTTCCTGT-3´
HLA-DRB1	5' -TTCCTGTGGCAGCCTAAGAG-3'	5' -AACCCCGTAGTTGTGTCTGC-3'
CD300E	5' -AGAGAAGGTGGAGAGGAATGG-3'	5' -AGGAAGATGGGAGGTGTGG-3'
CCR2	5'- CCCCAACGAGGCATAGA -3'	5'- AAGAGTCTCTGTCACCTGCG -3'
MMP9	5' -CGTCTTCCCCTTCACTTTCC-3	5' -CCCCACTTCTTGTCGCTGT-3'
BATF3	5' -AGGAAGGTCCGAAGGAGAGA-3'	5' -GAGGCACTGGCACAAAGTTC-3'
MX1	5' -CTGGGATTTTGGGGCTTT-3'	5' -GGGATGTGGCTGGAGATG-3'
OAS1	5' - TCAGAAATACCCCAGCCAAA-3'	5' -GAGCCACCCTTTACCACCTT-3'
TMPRSS2	5`-CCTCTAACTGGTGTGATGGCGT-3`	5`-TGCCAGGACTTCCTCTGAGATG-3´
ACTB	5`-CTGTCTGGCGGCACCACCAT-3'	5'-GCAACTAAGTCATAGTCCGC-3'
	ChIP Assays Primers	
PROMOTER	**Forward Primer**	**Reverse Primer**
IL1B Proximal	5`-TAGTTTGCTACTCCTTGCCCT-3´	5`-AGGAAAGGGGAAAAGAGTATTGGT-3´
IL1B Medial	5`-TGAATGAAGAAAAGTATGTGCATGT-3´	5`-AAATACTGGATTTTCCCACGTTAG-3´
IL6 Proximal	5`-AGCCTCAATGACGACCTAAGC-3	5`-GGGTGGGGCTGATTGGAAA-3`
IL6 Medial	5`-ACCTTCTTCATAATCCCAGGC-3´	5´-AGGCTAGAATTTAGCGTTCCAGT-3´
TNF Proximal	5`-ATGCTTGTGTGTCCCCAACT-3´	5`-CAGCGGAAAACTTCCTTGGTG-3´
TNF Medial	5`-GACCCAAACACAGGCCTCA-3`	5`-ACTAGAACTGGGAGGGGCTT-3´
TNF Distal	5`-GTCCAGGGCTATGGAAGTCG-3´	5`-CCCAGTGTGTGGCCATATCTT-3´

Real-Time Bioenergetic Analysis

514 Bioenergetic assays were carried out using an Agilent Seahorse XF HS Mini Analyzer. 10^5
515 MDDCs were adhered with Cell-Tak® to Seahorse plates and treated with stimuli of TLR3,
516 TLR7, and TLR8, as well as sonicated zymosan to activate the fungal pattern receptor dectin-
517 1 and TLR2, after a stabilization period. OCR and ECAR were analyzed according to the XF
518 Cell Mito Stress Test kit protocol in XF media under the experimental conditions and in
519 response to metformin, oligomycin, FCCP, and rotenone plus antimycin A.
520
521 **Aggresome Formation Assay**
522 The formation of aggresomes due to ER stress was assayed by flow cytometry fluorescence
523 using the Proteostat® aggresome detection kit of ENZO according to the manufacturer`s
524 instructions. The proteasome inhibitor MG132 was used as a positive control. MDDCs were
525 incubated under different conditions and then fixed, stained with Proteostat® dye and used for
526 the assay of fluorescence in a Gallios flow cytometer at 488 nm in the FL3 channel using the
527 Kaluza software version 1.1 for quantitative analysis (Beckman Coulter Life Sciences).
528
529 **Chromatin Immunoprecipitation (ChIP) Assay**
530 Chromatin immunoprecipitation assays were conducted using a rabbit mAb (Cell Signaling
531 Technology) against sXBP1 as previously reported [10]. Briefly, MDDCs were stimulated,
532 washed with PBS, and fixed with 1% formaldehyde. Cross-linking was terminated by 0.125 M
533 glycine. Crude nuclear extracts were collected by microcentrifugation. Chromatin sonication
534 was carried out using a Bioruptor device (Diagenode). The chromatin solution was precleared
535 by adding Protein A/G PLUS-Agarose for 30 min at 4°C under continuous rotation. After
536 elimination of the beads, mAb was added for overnight incubation at 4°C, and then Protein
537 A/G PLUS-Agarose was added and incubated for an additional period of 2 h at 4°C. Beads
538 were harvested by centrifugation at 4,000 x g and sequentially washed with lysis buffer high

539 salt, wash buffer, and elution buffer. Cross-links were reversed by heating at 67°C in a water
540 bath, and the DNA bound to the beads isolated by extraction with
541 phenol/chloroform/isoamylalcohol. Irrelevant Ab was used as control of binding specificity.
542 The sequences of the primers are shown in Table 1. Results are expressed as percentage of
543 input.
544
545 **Quantification and Statistical Analysis**
546 Data are represented as the mean ± SEM and were analyzed with the Prism 9.0 statistical
547 program. Repeated measures one-way and two-way ANOVA analyses were performed. When
548 data did not follow normal distribution nor had equal variances, log-transformation was applied
549 before analysis. Comparison between experimental groups was carried out using unpaired or
550 paired two-tailed Student's *t*-test and Wilkoxon signed-rank test, and Welch`s test. Statistical
551 details are shown in the Fig legends. Differences were considered significant for $p < 0.05$.
552
553 **ACKNOWLEDGMENTS**
554
555 José Javier Fernández is the recipient of a grant from *Junta de Castilla y León*. Cristina
556 Mancebo is the recipient of a pre-doctoral grant from the Valladolid Section of *Asociación*
557 *Española contra el Cáncer* (AECC). *Biobanco del Centro de Hemoterapia y Hemodonación*
558 *de Castilla y León* is thanked for providing buffy coats. Staff from the Intensive Care Unit of
559 *Hospital Clínico Universitario de Valladolid* is thanked for the effort devoted to patient follow-
560 up care and sample collection. BioRender.com software was used in some figures.
561
562 **AUTHOR CONTRIBUTIONS**
563

564 **Conceptualization:** Antonio Orduña, Juan Cubillos-Ruiz, Elena Bustamante, Nieves
565 Fernández, Mariano Sánchez Crespo.

566 **Data curation**: José J. Fernández, Sonsoles Garcinuño, Gabriel March, Luis Inglada, Antonio
567 Orduña, Juan Cubillos-Ruiz, Elena Bustamante, Mariano Sánchez Crespo.

568 **Formal analysis**: José J. Fernández, Yolanda Alvarez, Luis Inglada, Jesús Blanco, Antonio
569 Orduña, Elena Bustamante, Nieves Fernández, Mariano Sánchez Crespo.

570 **Funding acquisition**: Nieves Fernández, Mariano Sánchez Crespo.

571 **Investigation**: José J. Fernández, Cristina Mancebo, Sonsoles Garcinuño, Gabriel March,
572 Yolanda Alvarez, Sara Alonso, Luis Inglada, Jesús Blanco, Antonio Orduña, Olimpio Montero,
573 Tito A. Sandoval, Juan Cubillos-Ruiz, Elena Bustamante, Nieves Fernández, Mariano Sánchez
574 Crespo.

575 **Methodology**: José J. Fernández, Cristina Mancebo, Sonsoles Garcinuño, Gabriel March,
576 Yolanda Alvarez, Sara Alonso, Olimpio Montero, Elena Bustamante, Luis Inglada, Jesús
577 Blanco, Tito A. Sandoval, Antonio Orduña, Elena Bustamante.

578 **Project administration:** Nieves Fernández.

579 **Resources:** Nieves Fernández.

580 **Supervision:** Nieves Fernández, Mariano Sánchez Crespo.

581 **Validation:** Elena Bustamante, Luis Inglada, Jesús Blanco, Elena Bustamante, Nieves
582 Fernández.

583 **Visualization:** José J. Fernández, Nieves Fernández, Mariano Sánchez Crespo.

584 **Writing – original draft:** Luis Inglada, Jesús Blanco, Tito A. Sandoval, Juan Cubillos-Ruiz,
585 Nieves Fernández, Mariano Sánchez Crespo.

586 **Writing – review & editing:** Luis Inglada, Jesús Blanco, Tito A. Sandoval, Juan Cubillos-
587 Ruiz, Elena Bustamante, Nieves Fernández, Mariano Sánchez Crespo.

588

589 **FUNDING**

590

591 This study was funded by *Fondo COVID-19 del Instituto de Salud Carlos III/Junta de Castilla*
592 *y León* (N.F.). European Commission-NextGenerationEU, through CSIC's Global Health
593 Platform (PTI Salud Global) (project SGL2103016) (M.S.C.). *Plan Nacional de Salud y*
594 *Farmacia* Grant SAF2017-83079-R and Grant PID2020-113751RB-I00 funded by
595 MCIN/AEI/ 10.13039/501100011033 (M.S.C.). *Junta de Castilla y León/Fondo Social*
596 *Europeo* Grants CSI035P17 (M.S.C.) and VA175P20 (N.F.). *Proyecto* SEAHORSE
597 INFRARED: IR2020-1-UVA05 (JCyL). The funders had no role in study design, data
598 collection and analysis, decision to publish, or preparation of the manuscript.

599

600

601 **REFERENCES**

602

603 1. Fajgenbaum DC, June CH. Cytokine storm. N Engl J Med. 2020;383: 2255-2273.

604 2. Riva G, Nasillo V, Tagliafico E, Trenti T, Comoli P, Luppi M. COVID-19: more than a
605 cytokine storm. Crit. Care. 2020;24: 549.

606 3. Hetz C, Zhang K, Kaufman RJ. Mechanisms, regulation and functions of the unfolded protein
607 response. Nat Rev Mol Cell Biol. 2012;13: 89-102.

608 4. Bettigole SE, Glimcher LH. Endoplasmic reticulum stress in immunity. Annu Rev Immunol.
609 2015;33: 107-138.

610 5. Chen X, Cubillos-Ruiz, JR. Endoplasmic reticulum stress signals in the tumour and its
611 microenvironment. Nat Rev Cancer. 2021;21: 71-88.

612 6. Calfon M, Zeng H, Urano F, Till JH, Hubbard SR, Harding HP, et al. IRE1 couples
613 endoplasmic reticulum load to secretory capacity by processing the XBP-1 mRNA.
614 Nature. 2002;415: 92-96.

615 7. Chopra S, Giovanelli P, Alvarado-Vazquez PA, Alonso S, Song M, Sandoval TA, et al.
616 IRE1α-XBP1 signaling in leukocytes controls prostaglandin biosynthesis and pain.
617 Science. 2019;365(6450): eaau6499.

618 8. Martinon F, Chen X, Lee AH, Glimcher LH. TLR activation of the transcription factor XBP1
619 regulates innate immune responses in macrophages. Nat Immunol. 2011;11: 411-418.

620 9. Zeng L, Liu YP, Sha H, Chen H, Qi L, Smith JA. XBP-1 couples endoplasmic reticulum
621 stress to augmented IFN-β induction via a *cis*-acting enhancer in macrophages. J
622 Immunol. 2010;185: 2324-2330.

623 10. Márquez S, Fernández JJ, Terán-Cabanillas E, Herrero C, Alonso S, Azogil A, et al.
624 Endoplasmic reticulum stress sensor IRE1α enhances IL-23 expression by human
625 dendritic cells. Front Immunol. 2017;8: 639.

626 11. Mogilenko DA, Haas JT, L'homme L, Fleury S, Quemener S, Levavasseur, et al. Metabolic
627 and innate immune cues merge into a specific inflammatory response via the UPR. Cell.
628 2019;177: 1201-1216.

629 12. Keestra-Gounder AM, Byndloss MX, Seyffert N, Young BM, Chávez-Arroyo A, Tsai AY,
630 et al. NOD1 and NOD2 signalling links ER stress with inflammation. Nature. 2016;532:
631 394-397.

632 13. Qiu Q, Zheng Z, Chang L, Zhao YS, Tan C, Dandekar A, et al. Toll-like receptor-mediated
633 IRE1α activation as a therapeutic target for inflammatory arthritis. EMBO J. 2013;32:
634 2477-2490.

635 14. Rosen DA, Seki SM, Fernández-Castañeda A, Beiter RM, Eccles JD, Woodfolk JA, et al.
636 Modulation of the sigma-1 receptor-IRE1 pathway is beneficial in preclinical models
637 of inflammation and sepsis. Sci Transl Med. 2019;11(478):eaau5266.

638 15. Sule G, Abuaita BH, Steffes PA, Fernandes AT, Estes SK, Dobry C, et al. Endoplasmic
639 reticulum stress sensor IRE1α propels neutrophil hyperactivity in lupus. J Clin Invest.
640 2021;131(7):e137866.

641 16. Prasad, V, Suomalainen M, Jasiqi Y, Hemmi S, Hearing P, Hosie L, et al. The UPR sensor
642 IRE1α and the adenovirus E3-19K glycoprotein sustain persistent and lytic infections.
643 Nat Commun. 2020;11: 1997.

644 17. Prasad V, Greber UF. The endoplasmic reticulum unfolded protein response - homeostasis,
645 cell death and evolution in virus infections. FEMS Microbiol Rev. 2021;45: fuab016.

646 18. Hrincius ER, Liedmann S, Finkelstein D, Vogel P, Gansebom S, Samarasinghe AE, et al.
647 Acute lung injury results from innate sensing of viruses by an ER stress pathway. Cell
648 Rep. 2015;11: 1591-1603.

649 19. Rosa-Fernandes L, Lazari LC, Macedo da Silva J, de Morais Gomes V, Guaragna Machado
650 RR, Ferreira dos Santos A, et al. SARS-CoV-2 activates ER stress and unfolded protein
651 response. bioRxiv. 2021;doi: https://doi.org/10.1101/2021.06.21.449284.

652 20. Liu N, Jiang C, Cai P, Shen Z, Sun W, Xu H, et al. Single-cell analysis of COVID-19,
653 sepsis, and HIV infection reveals hyperinflammatory and immunosuppressive
654 signatures in monocytes. Cell Rep. 2021;37: 109793.

655 21. Blanco-Melo D, Nilsson-Payant BE, Liu WC, Uhl S, Hoagland D, Møller R, et al.
656 Imbalanced host response to SARS-CoV-2 drives development of COVID-19. Cell.
657 2020;81: 1036–1045.

658 22. Xu X, Han M, Li T, Sun W, Wang D, Fu B, et al. Effective treatment of severe COVID-19
659 patients with tocilizumab. Proc Natl Acad Sci USA. 2020;117: 10970-10975.

660 23. Acosta-Alvear D, Zhou Y, Blais A, Tsikitis M, Lents NH, Arias C, et al. XBP1 controls
661 diverse cell-type and condition-specific transcriptional regulatory networks. Mol Cell.
662 2007;27: 53-66.

663 24. Cubillos-Ruiz JR, Silberman PC, Rutkowski MR, Chopra S, Perales-Puchalt A, Song M, et
664 al. ER stress sensor XBP1 controls anti-tumor immunity by disrupting dendritic cell
665 homeostasis. Cell. 2015;161: 1527-1538.
666

667 25. Song M, Sandoval TA,Chae CS, Chopra S, Tan C, Rutkowski MR, et al. IRE1α-XBP1
668 controls T cell function in ovarian cancer by regulating mitochondrial activity. Nature.
669 2018;562: 423-428.

670 26. Echavarría-Consuegra L, Cook GM, Busnadiego I, Lefèvre C, Keep S, Brown K, et al.
671 Manipulation of the unfolded protein response: A pharmacological strategy against
672 coronavirus infection. PLoS Pathog. 2021;17(6):e1009644.

673 27. Nguyen LC, Yang D, Nicolaescu V, Best TJ, Gula H, Saxena D, et al. Cannabidiol inhibits
674 SARS-CoV-2 replication through induction of the host ER stress and innate immune
675 responses. Sci Adv. 2022 Jan 20:6110. Epub ahead of print. PMID: 35050692.
676
677 28. van der Made CI, Simons A, Schuurs-Hoeijmakers J, van den Heuvel G, Mantere T, Kersten
678 S, et al. Presence of genetic variants among young men with severe COVID-19. JAMA.
679 2020;324: 1-11.

680 29. Rodríguez M, Domingo E, Alonso S, Frade JG, Eiros J, Sánchez Crespo M, et al. The
681 unfolded protein response and the phosphorylations of activating transcription factor 2
682 in the trans-activation of *IL23A* promoter produced by β-glucans. J Biol Chem.
683 2014;289: 22942-22957.

684 30. Turini ME, DuBois RN. Cyclooxygenase-2: A Therapeutic Target. Annu Rev Med.
685 2002;53: 35-57.

686 31. Codo AC, Davanzo GG, Monteiro LB, de Souza GF, Muraro SP, Virgilio-da-Silva JV, et
687 al. Elevated glucose levels favor SARS-CoV-2 infection and monocyte response
688 through a HIF-1α/glycolysis-dependent axis. Cell Metab. 2020;32: 437-446.

689 32. O'Carroll SM, O'Neill LAJ. Targeting immunometabolism to treat COVID-19. Immunother
690 Adv. 2021;1: ltab013.

691 33. Song R, Gao Y, Dozmorov I, Malladi V, Saha I, McDaniel MM, et al. IRF1 governs the
692 differential interferon-stimulated gene responses in human monocytes and
693 macrophages by regulating chromatin accessibility. Cell Rep. 2021;34: 108891.

694 34. Hoffmann M, Kleine-Weber H, Schroeder S, Krüger N, Herrler T, Erichsen S, et al. SARS-
695 CoV-2 cell entry depends on ACE2 and TMPRSS2 and is blocked by a clinically proven
696 protease inhibitor. Cell. 2020;181: 271-280.

697 35. Andolfo I, Russo R, Lasorsa VA, Cantalupo S, Rosato BE, Bonfiglio F, et al. Common
698 variants at 21q22.3 locus influence *MX1* and *TMPRSS2* gene expression and
699 susceptibility to severe COVID-19. iScience. 2021;24: 102322.

700 36. Hadjadj J, Yatim N, Barnabei L, Corneau A, Boussier J, Smith N, et al. Impaired type I
701 interferon activity and inflammatory responses in severe COVID-19 patients. Science.
702 2020;369: 718-724.

703 37. Karki R, Sharma BR, Tuladhar S, Williams EP, Zalduondo L, Samir P, et al. Synergism of
704 TNF-α and IFN-γ triggers inflammatory cell death, tissue damage, and mortality in
705 SARS-CoV-2 infection and cytokine shock syndromes. Cell. 2021;184: 149-168.e17.

706 38. Huang KJ, Su IJ, Theron M, Wu YC, Lai SK, Liu CC, et al. An interferon-γ-related cytokine
707 storm in SARS patients. J Med Virol. 2005;75: 185-194.

708 39. Broggi A, Ghosh S, Sposito B, Spreafico R, Balzarini F, Lo Cascio A, et al. Type III
709 interferons disrupt the lung epithelial barrier upon viral recognition. Science. 2020;369:
710 706-712.

711 40. Gao DK, Salomonis N, Henderlight M, Woods C, Thakkar K, Grom AA, et al. IFN-γ is
712 essential for alveolar macrophage driven pulmonary inflammation in macrophage
713 activation syndrome. JCI Insight. 2021;27: 147593.

714 41. Verma AK, Bauer C, Palani S, Metzger DW, Sun K. IFN-γ drives TNF-α hyperproduction
715 and lethal lung inflammation during antibiotic treatment of postinfluenza
716 staphylococcus aureus pneumonia. J Immunol. 2021;207: 1371-1376.

717 42. Mimura N, Fulciniti M, Gorgun G, Tai YT, Cirstea D, Santo L, et al. Blockade of XBP1
718 splicing by inhibition of IRE1α is a promising therapeutic option in multiple myeloma.
719 Blood. 2012;119: 5772-5781.

720 43. Krawczyk CM, Holowka T, Sun J, Blagih J, Amiel E, DeBerardinis RJ, et al. Toll-like
721 receptor-induced changes in glycolytic metabolism regulate dendritic cell activation.
722 Blood. 2010;115: 4742-4749.

723 44. Xian H, Liu Y, Rundberg Nilsson A, Gatchalian R, Crother TR, Tourtellotte WG, et al.
724 Metformin inhibition of mitochondrial ATP and DNA synthesis abrogates NLRP3
725 inflammasome activation and pulmonary inflammation. Immunity. 2021;54: 1463-
726 1477.e11.

727 45. Kelly B, Tannahill GM, Murphy MP, O'Neill LA. Metformin inhibits the production of
728 reactive oxygen species from NADH:ubiquinone oxidoreductase to limit induction of
729 interleukin-1β (IL-1β) and boosts interleukin-10 (IL-10) in lipopolysaccharide (LPS)-
730 activated macrophages. J Biol Chem. 2015;290: 20348-20359.

731 46. Baselski VS, Wunderink RG. Bronchoscopic diagnosis of pneumonia. Clin Microbiol Rev.
732 1994;7: 533-558.

733 47. Shin YM, Oh YM, Kim MN. Usefulness of quantitative endotracheal aspirate cultures in
734 intensive care unit patients with suspected pneumonia. J Korean Med Sci. 2011;26: 865-
735 869.

736 48. Pickens C, Wunderink RG, Qi C, Mopuru H, Donnelly H, Powell K, et al. A multiplex
737 polymerase chain reaction assay for antibiotic stewardship in suspected pneumonia.
738 Diagn Microbiol Infect Dis. 2020;98: 115179.

739 49. Zhou Z, Ren L, Zhang L, Zhong J, Xiao Y, Jia Z, et al. Heightened innate immune responses
740 in the respiratory tract of COVID-19 patients. Cell Host Microbe. 2020;27: 883-890.

741 50. Liao M, Liu Y, Yuan J, Wen Y, Xu G, Zhao J, et al. Single-cell landscape of
742 bronchoalveolar immiune cells in patients with COVID-19. Nat. Med. 2020;26: 842-
743 844.

744 51. Szabo PA, Dogra P, Gray JI, Wells SB, Connors TJ, Weisberg SP, et al. Developmental
745 regulation of effector and resident memory T cell generation during pediatric viral
746 respiratory tract infection. J Immunol. 2018;201: 432-439.

747 52. Connors TJ, Baird JS, Yopes MC, Zens KD, Pethe K, Ravindranath TM, et al.
748 Developmental regulation of effector and resident memory T cell generation during
749 pediatric viral respiratory tract Infection. J Immunol. 2018;201: 432-439.

750 53. Connors TJ, Ravindranath TM, Bickham KL, Gordon CL, Zhang F, Levin B, et al. Airway
751 CD8(+) T cells are associated with lung injury during infant viral respiratory tract
752 infection. Am J Respir Cell Mol Biol. 2016;54: 822-830.

753 54. Sarma A, Christenson SA, Byrne A, Mick E, Pisco AO, DeVoe C, et al. Tracheal aspirate
754 RNA sequencing identifies distinct immunological features of COVID-19 ARDS. Nat
755 Commun. 2021;12:5152.

756 55. Sinha P, Matthay MA, Calfee CS. Is a "Cytokine Storm" relevant to COVID-19? JAMA
757 Intern Med. 2020;180:1152-1154.

758 56. Kox M, Waalders NJB, Kooistra EJ, Gerretsen J, Pickkers P. Cytokine levels in critically
759 Ill patients with COVID-19 and other conditions. JAMA. 2020;324:1565-1567.

760 57. Lenze EJ, Mattar C, Zorumski CF, Stevens A, Schweiger J, Nicol GE, et al. Fluvoxamine
761 vs placebo and clinical deterioration in outpatients with symptomatic COVID-19: A
762 randomized clinical trial. JAMA. 2020;324: 2292-2300.

763 58. Reis G, dos Santos Moreira-Silva EA, Medeiros Silva DC, Thabane L, Cruz Milagres A,
764 Santiago Ferreira T, et al. Effect of early treatment with fluvoxamine on risk of
765 emergency care and hospitalisation among patients with COVID-19: the TOGETHER
766 randomised, platform clinical trial. Lancet Glob Health 2022 Jan;10(1):e42-e51.
767
768 59. Shi S, Blumenthal A, Hickey CM, Gandotra S, Levy D, Ehrt S. Expression of many
769 immunologically important genes in *Mycobacterium tuberculosis*-infected
770 macrophages is independent of both TLR2 and TLR4 but dependent on IFN-αβ receptor
771 and STAT1. J Immunol. 2005;175: 3318-3328.

772 60. Michelucci A, Cordes T, Ghelfi J, Pailot A, Reiling N, Goldmann O, et al. Immune-
773 responsive gene 1 protein links metabolism to immunity by catalyzing itaconic acid
774 production. Proc Natl Acad Sci USA. 2013;110: 7820-7825.

775 61. Hooftman A, Angiari S, Hester S, Corcoran SE, Runtsch MC, Ling C, et al. The
776 immunomodulatory metabolite itaconate modifies NLRP3 and inhibits inflammasome
777 activation. Cell Metab. 2020;32: 468-478.

778 62. Giamarellos-Bourboulis EJ, Netea MG, Rovina N, Akinosoglou K, Antoniadou A,
779 Antonakos N, et al. Complex immune dysregulation in COVID-19 patients with severe
780 respiratory failure. Cell Host Microbe. 2020;27: 992-1000.e3.

781 63. Rappe JCF, Finsterbusch K, Crotta S, Mack M, Priestnall SL, Wack A. A TLR7 antagonist
782 restricts interferon-dependent and -independent immunopathology in a mouse model of
783 severe influenza. J Exp Med. 2021;218: e20201631.

784 64. Li Y, Chen M, Cao H, Zhu Y, Zheng J, Zhou H. Extraordinary GU-rich single-strand RNA
785 identified from SARS coronavirus contributes an excessive innate immune response.
786 Microbes Infect. 2013;15: 88-95.

787 65. Campbell GR, To RK, Hanna J, Spector SA. SARS-CoV-2, SARS-CoV-1, and HIV-1
788 derived ssRNA sequences activate the NLRP3 inflammasome in human macrophages
789 through a non-classical pathway. iScience. 2021;24: 102295.

790 66 Fallerini C, Daga S, Mantovani S, Benetti E, Picchiotti N, Francisci D, et al. Association of
791 Toll-like receptor 7 variants with life-threatening COVID-19 disease in males: findings
792 from a nested case-control study. Elife. 2021;10: e67569.

793 67. Zhang Q, Bastard P, Liu Z, Le Pen J, Moncada-Velez M, Chen J, et al. Inborn errors of type
794 I IFN immunity in patients with life-threatening COVID-19. Science. 2020;370:
795 eabd4570.

796 68. Ito T, Amakawa R, Kaisho T, Hemmi H, Tajima K, Uehira K, et al. Interferon-α and
797 interleukin-12 are induced differentially by Toll-like receptor 7 ligands in human blood
798 dendritic cell subsets. J Exp Med. 2002;195: 1507-1512.

799 69. Olson GS, Murray TA, Jahn AN, Mai D, Diercks AH, Gold ES, et al. Type I interferon
800 decreases macrophage energy metabolism during mycobacterial infection. Cell Rep.
801 2021;35: 109195.

802 70. Thwe PM, Fritz DI, Snyder JP, Smith PR, Curtis KD, O'Donnell A, et al. Syk-dependent
803 glycolytic reprogramming in dendritic cells regulates IL-1β production to β-glucan
804 ligands in a TLR-independent manner. J Leukoc Biol. 2019;106: 1325-1335.

805 71. Fan E, Del Sorbo L, Goligher EC, Hodgson CL, Munshi L, Walkey AJ, et al. An Official
806 American Thoracic Society/European Society of Intensive Care Medicine/Society of

807 Critical Care Medicine Clinical Practice Guideline: Mechanical Ventilation in Adult
808 Patients with Acute Respiratory Distress Syndrome. Am J Respir Crit Care Med.
809 2017;195: 1253-1263.

810

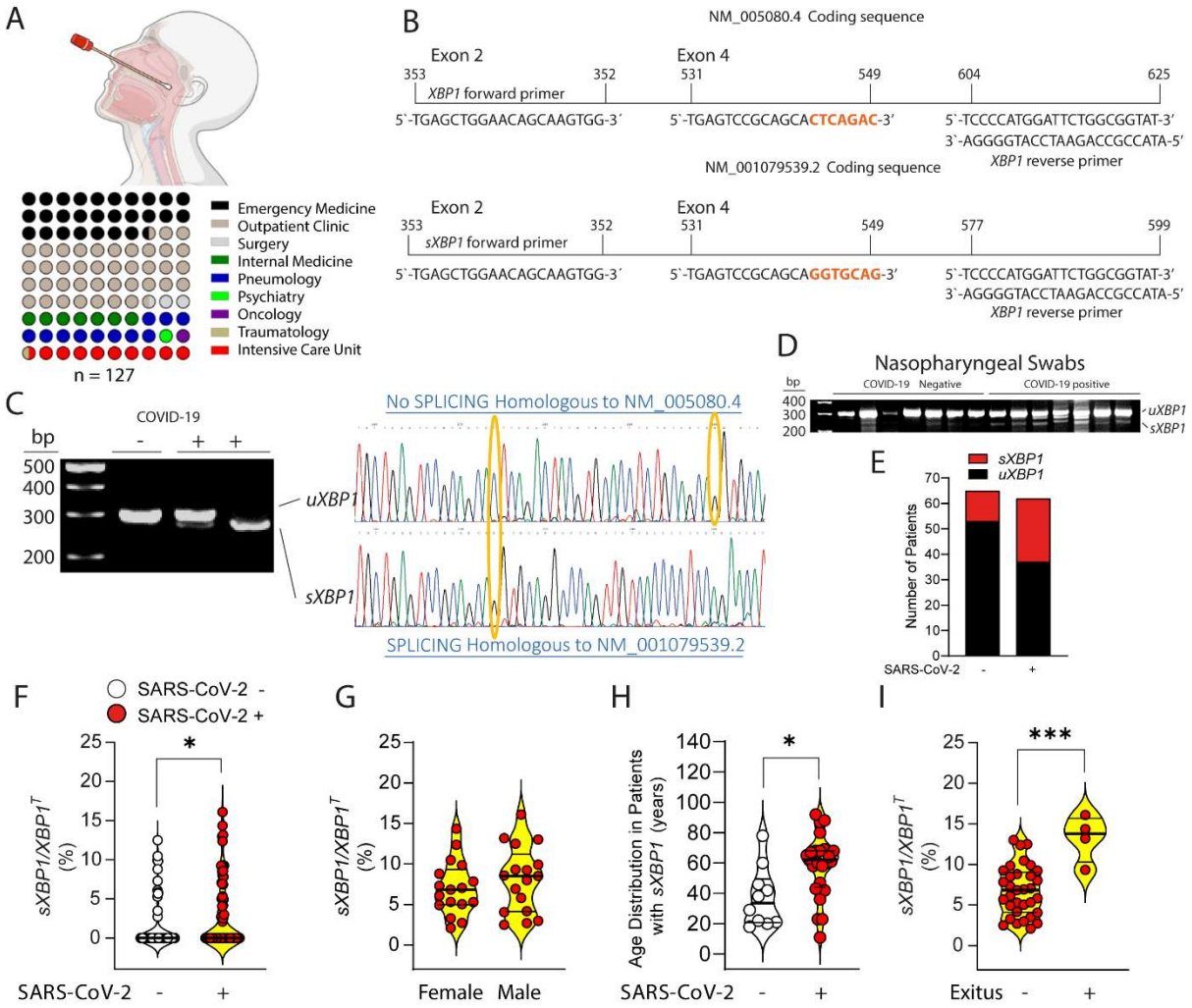

Fig 1. Sequences of *XBP1* mRNA transcripts and analysis of RT-PCR products in nasopharyngeal samples. (A) Medical departments involved in the obtention of nasopharyngeal swabs. (B) The splicing of 26 nucleotides in NM_005080.4 sequence generates the 531-549 sequence in NM_001079539.2. The position of primers, including the reverse primer spanning the spliced sequence is shown. (C) Agarose gel electrophoresis and sequencing of the amplicons obtained by RT-PCR with XBP1 primers showing the migration of the spliced (*sXBP1*) and unspliced products (*uXBP1*). (D) The electrophoretic pattern of *XBP1* in a series of samples from COVID-19 negative and positive patients is shown. The presence of three bands in some cases is due to the formation of heteroduplexes. (E) Distribution of patients according to the presence or absence of *sXBP1* in SARS-CoV-2 negative and positive patients. (F) Quantitation of *sXBP1* versus total *XBP1* ($XBP1^T$) in COVID-19 positive and negative samples. (G) Quantitation of *sXBP1* versus total *XBP1* in male and female SARS-CoV-2 positive patients. (H) Age distribution of patients with *sXBP1*. (I) Quantitation of *sXBP1* versus total *XBP1* in SARS-CoV-2 positive according to the outcome. *p < 0.05, ***p<0.005, paired or unpaired (two-tail) *t* test.

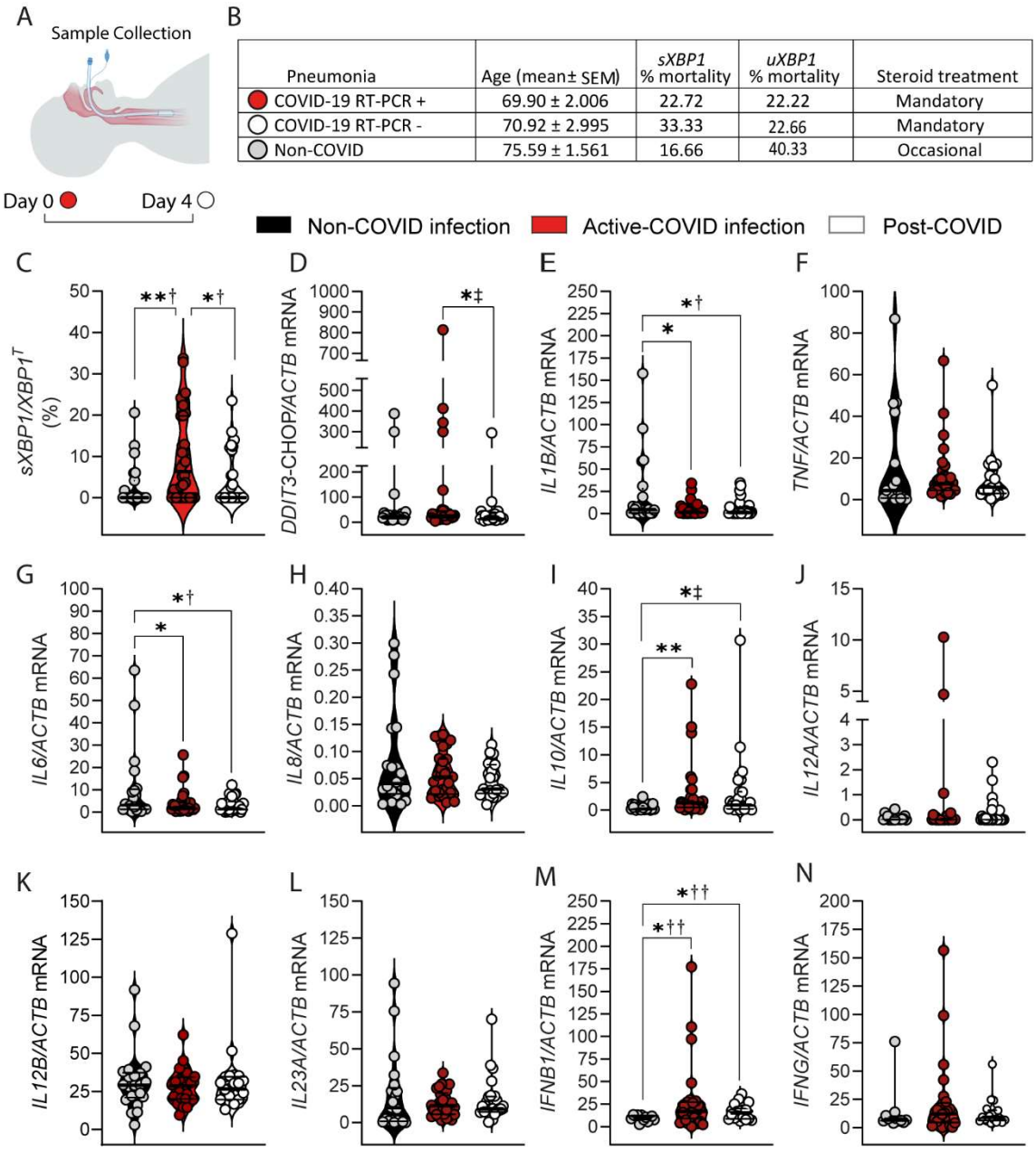

Fig 2. Expression of the mRNA of *XBP1*, *DDIT3*/CHOP, and cytokines in BAAs of patients under mechanical ventilation in ICU. (A) Scheme of sample collection. (B) Stratification of patients according to non-COVID-19, active COVID-19, and non-active COVID-19 infection. (C) *sXBP1* expression in the different cohorts. Results are expressed as mean ± SEM. †Ordinary one-way ANOVA with the Tukey's multiple comparisons test. *p < 0.05. *** p < 0.005. (D) Expression of the mRNA de *DDIT3*/CHOP. ‡Kruskal-Wallis *U* test. (E-N) Expression of the mRNA encoding *IL1B*, *TNF*, *IL6*, *IL8, IL10, IL12A, IL12B, IL23A, IFNB1,* and *IFNG* in BAAs. Data are presented as mean ± SEM. *p < 0.05, **p < 0.01, ***p<0.005. †Ordinary one-way ANOVA. ‡Kruskal-Wallis *U* test. ††Welch and Brown-Forsythe ANOVA test.

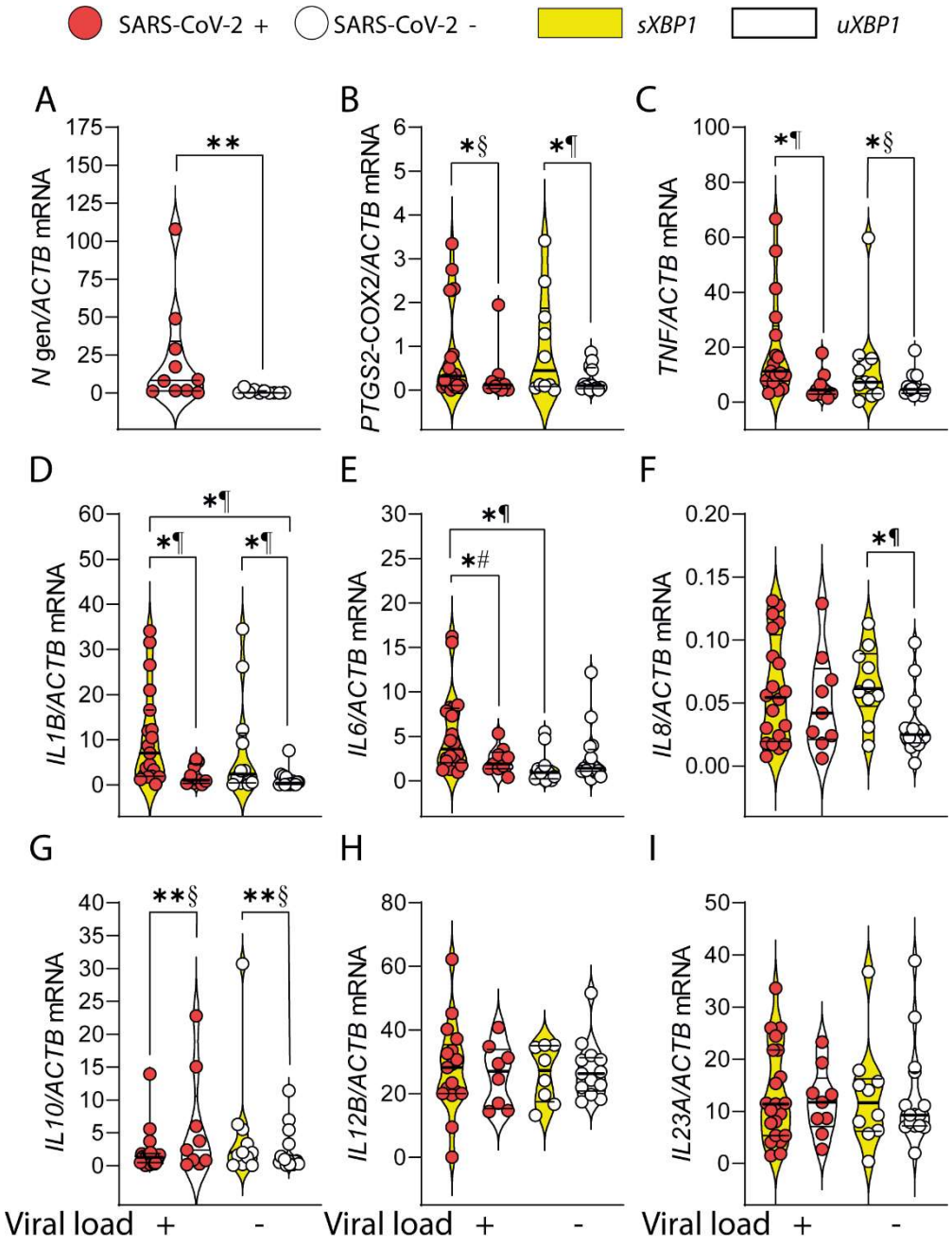

Fig 3. Association of *sXBP1* splicing and viral replication with cytokine expression in BAAs. (A) Viral load in samples obtained at the time of SARS-CoV-2 positive and negative tests. Data are presented as mean ± SEM. **p < 0.01. Unpaired two-tailed Student's *t* test. (B-I) Patients were stratified in cohorts according to the presence of *sXBP1* and the presence or absence of viral load as deemed from RT-PCR test for SARS-CoV-2 infection. The mRNA of *PTGS2* and various cytokines was assayed in the extracted RNA and the statistical significance of the results was assayed using ordinary one-way ANOVA with Tukey´s post-hoc multiple comparison test. Data are presented as mean ± SEM. *p<0.05, **p<0.01, ***p<0.005. §One-sample Wilkoxon signed rank test. ¶Unpaired (two-tail) *t* test. #Welch`s test.

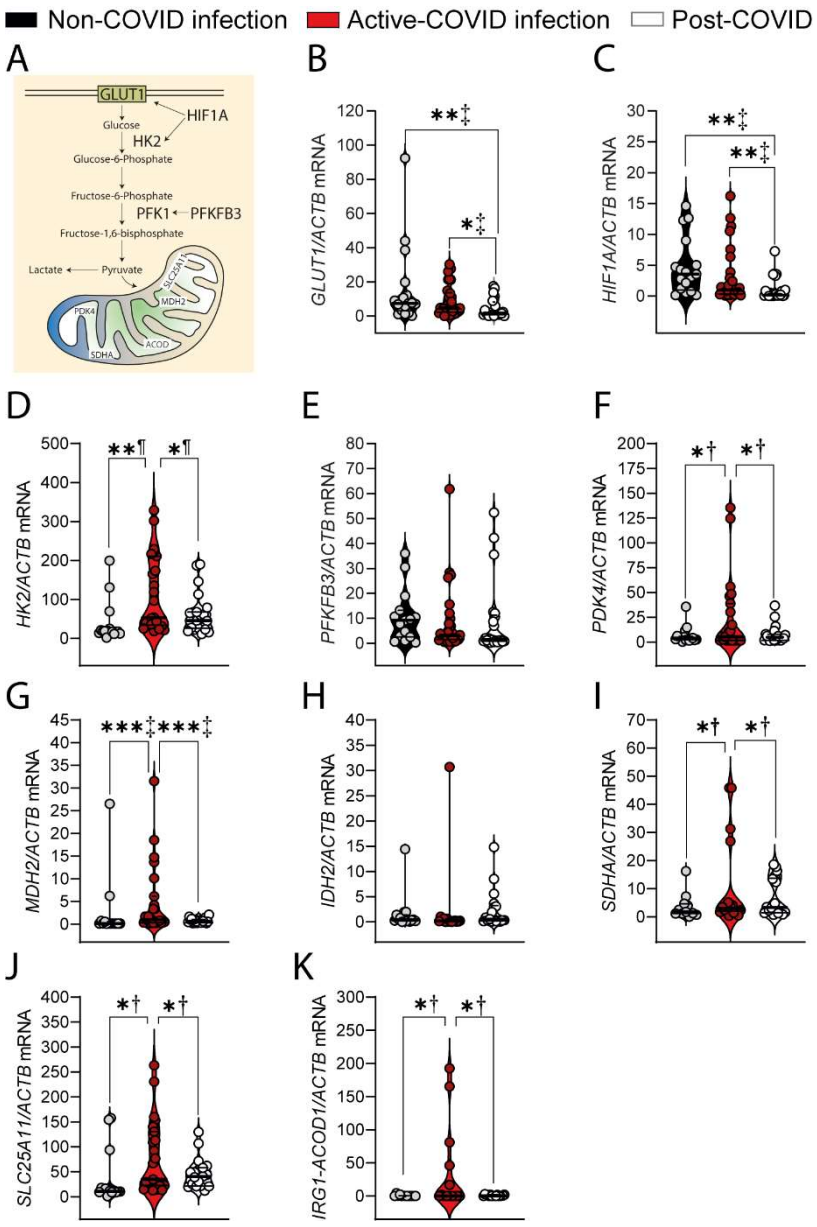

Fig 4. Expression of enzymes involved in glycolysis and mitochondrial proteins. (A) Diagram of glycolytic and mitochondrial proteins assayed in BAAs. (B-K) BAAs of patients with controlled respiration were used for RNA extraction and RT-PCR assay of mRNA expression of genes encoding for proteins involved in glycolysis, response to hypoxia, and mitochondrial function. *GLUT1*, glucose transporter 1. *HIF1A,* hypoxia-inducible factor 1α. *HK2*, hexokinase 2. *PFKB3*, 6-phosphofructo-2-kinase/fructose-2,6-biphosphatase. *PDK4*, pyruvate dehydrogenase kinase. *MDH2*, malate dehydrogenase 2. *IDH2*, isocitrate dehydrogenase 2. *SDHA*, succinate dehydrogenase protein subunit A. *SLC25A11*, mitocondrial 2-oxoglutarate-malate carrier. *IRG1*-ACOD1, immunoresponsive gene 1-aconitate decarboxylase. Data are presented as mean ± SEM. *p < 0.05, **p < 0.01, ***p<0.005. ‡Kruskal-Wallis *U* test. †Ordinary one-way ANOVA. ¶Paired or unpaired (two-tail) *t* test.

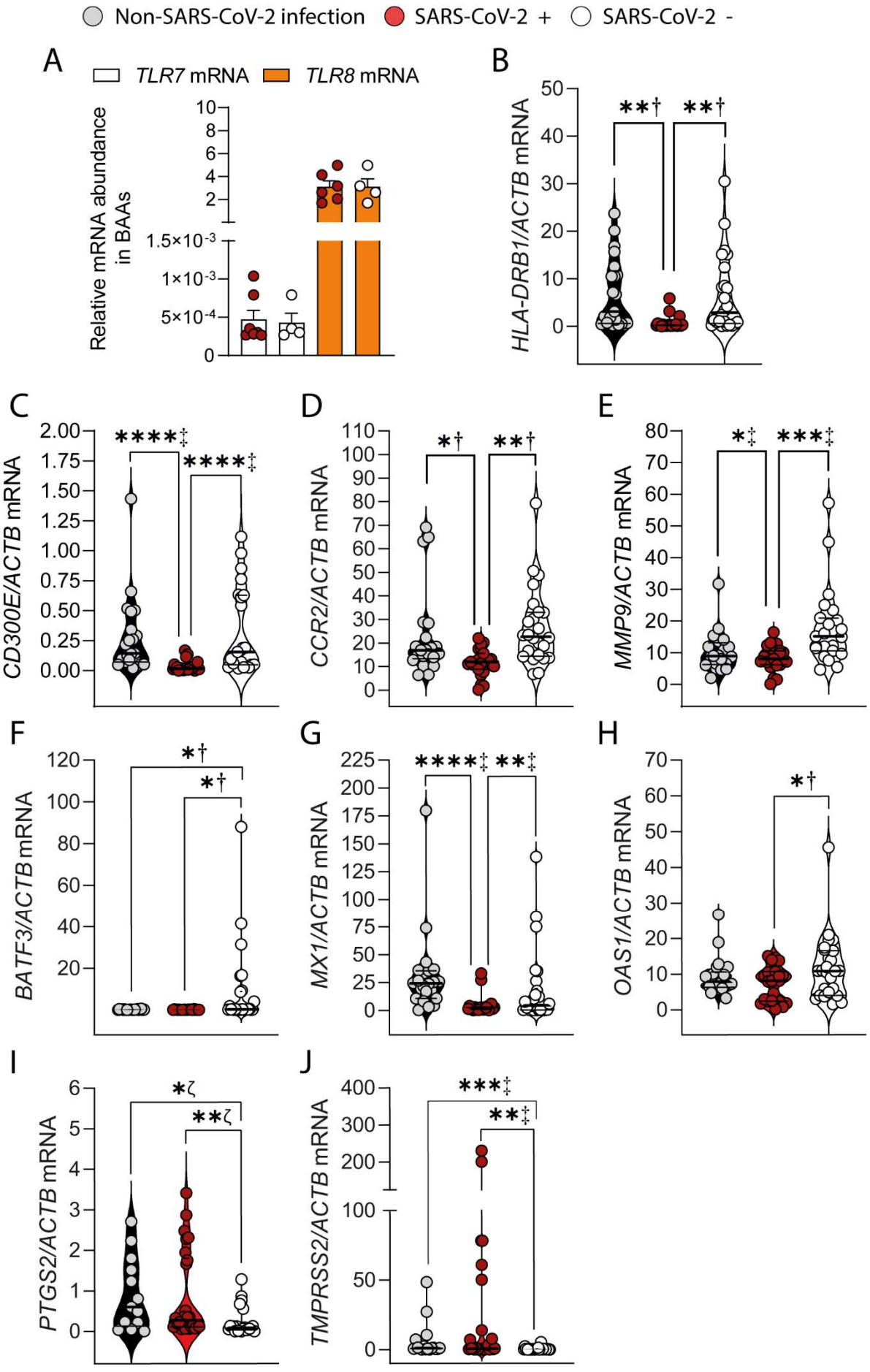

Fig 5. Expression of genes involved in monocytic-lineage differentiation in BAAs. (A) Expression of the mRNA encoding the receptors TLR7 and TLR8 in patients with active SARS-CoV-2 infection and after negative tests. (B-F) Expression of monocyte-differentiation markers in BAAs of non-COVID-19, COVID-19, and post-COVID-19 infection. (G-H) Expression of the ISG *MX1* and *OAS1* mRNA. (I) Expression of the mRNA encoding *PTGS2*/COX2. (J) Expression of the mRNA encoding the transmembrane serine protease *TMPRSS2*. Data are presented as mean ± SEM. *p < 0.05, **p < 0.01, ***p<0.005. †Ordinary one-way ANOVA. ‡Kruskal-Wallis *U* test. ζHolm-Sidak`s multiple comparison test.

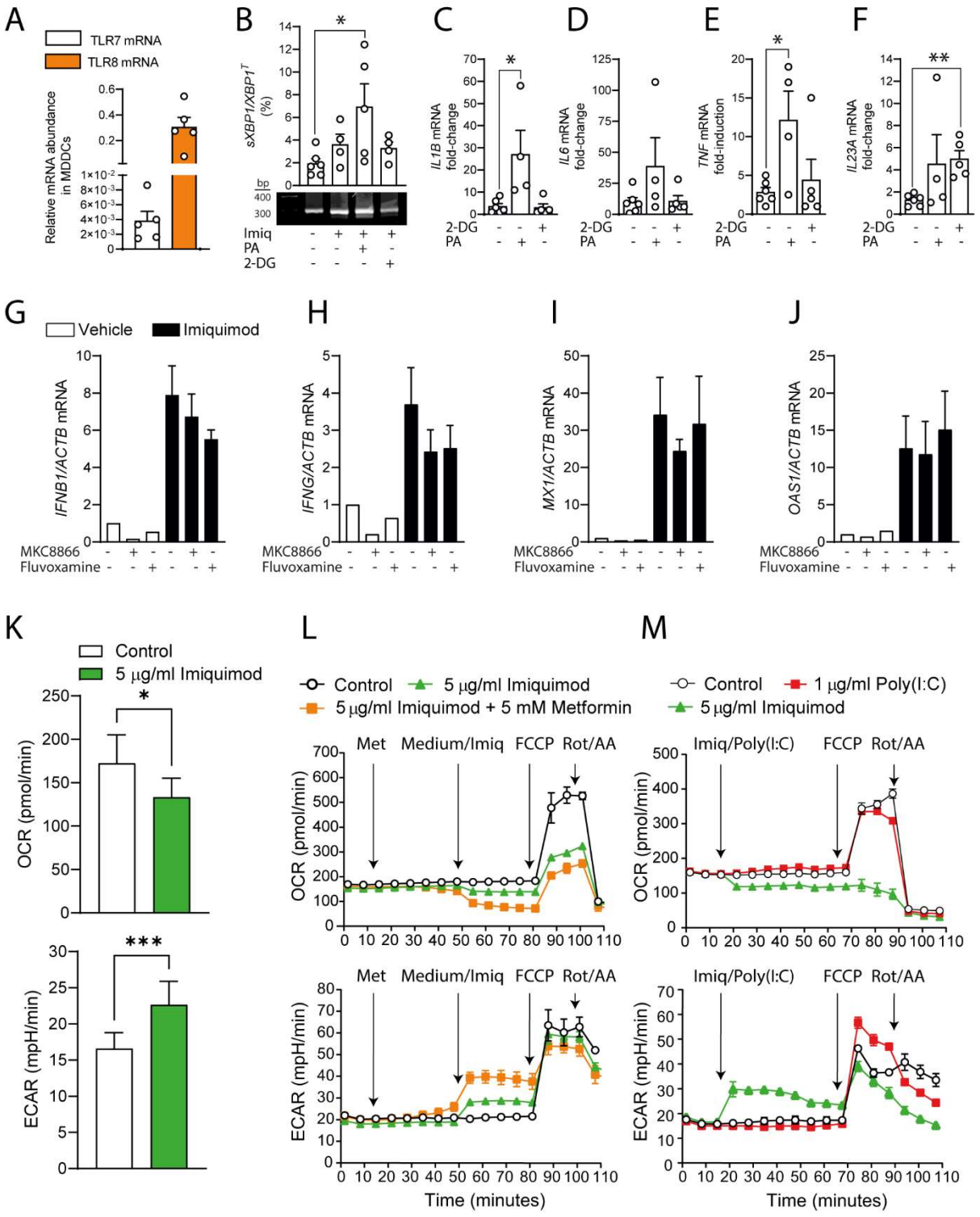

Fig 6. Expression of TLR7 and TLR8 receptors in MDDCs and response to the TLR7 agonist imiquimod. (A) Expression of the mRNA encoding TLR7 and TLR8 in MDDCs. (B) Effect of 5 µg/ml imiquimod on *sXBP1* in the presence and absence of 0.5 mM palmitate (PA) and 10 mM 2-deoxyglucose (2-DG). MDDCs were incubated for one hour in the presence of the indicated additions and then stimulated with imiquimod for 1 hour. At the end of this time, the RNA was extracted and used for the assay of *sXBP1*. (C-F) Effect of imiquimod on the expression of the mRNA encoding *IL1B*, *TNF*, *IL6*, and *IL23A*. The stimulation with

imiquimod was maintained for four hours before RNA extraction. Data are presented as mean ± SEM. *p < 0.05, **p < 0.01. (G-J) Effect of MKC8866 and fluvoxamine on the expression of the mRNA encoding *IFNB1*, *IFNG*, *MX1*, and *OAS1*. MDDCs were preincubated with 10 μM MKC8866 and 20 μM fluvoxamine for one hour and then stimulated with 5 μg/ml imiquimod for 4 hours. At the end of this time, the RNA was extracted and used for mRNA assay. (K) Effect of imiquimod on O_2 consumption rate (OCR) and glycolysis assayed as extracellular acidification rate (ECAR). Data are presented as mean ± SEM. *p < 0.05, ***p < 0.005, paired, (two-tail) Student's *t* test. (L) Seahorse real-time metabolic analysis of one experiment where MDDCs were stimulated with imiquimod and then treated with 2 μM FCCP (an uncoupler of oxidative phosphorylation) to estimate maximal respiratory rate, and the combination 0.5 μM rotenone/antimycin (Rot/AA) to inhibit complex I and complex III of the mitochondrial electron transport chain. Where indicated, metformin was used to inhibit complex I activity. (M) MDDCs were treated with imiquimod or with poly(I:C) to show the effect of a TLR3 agonist.

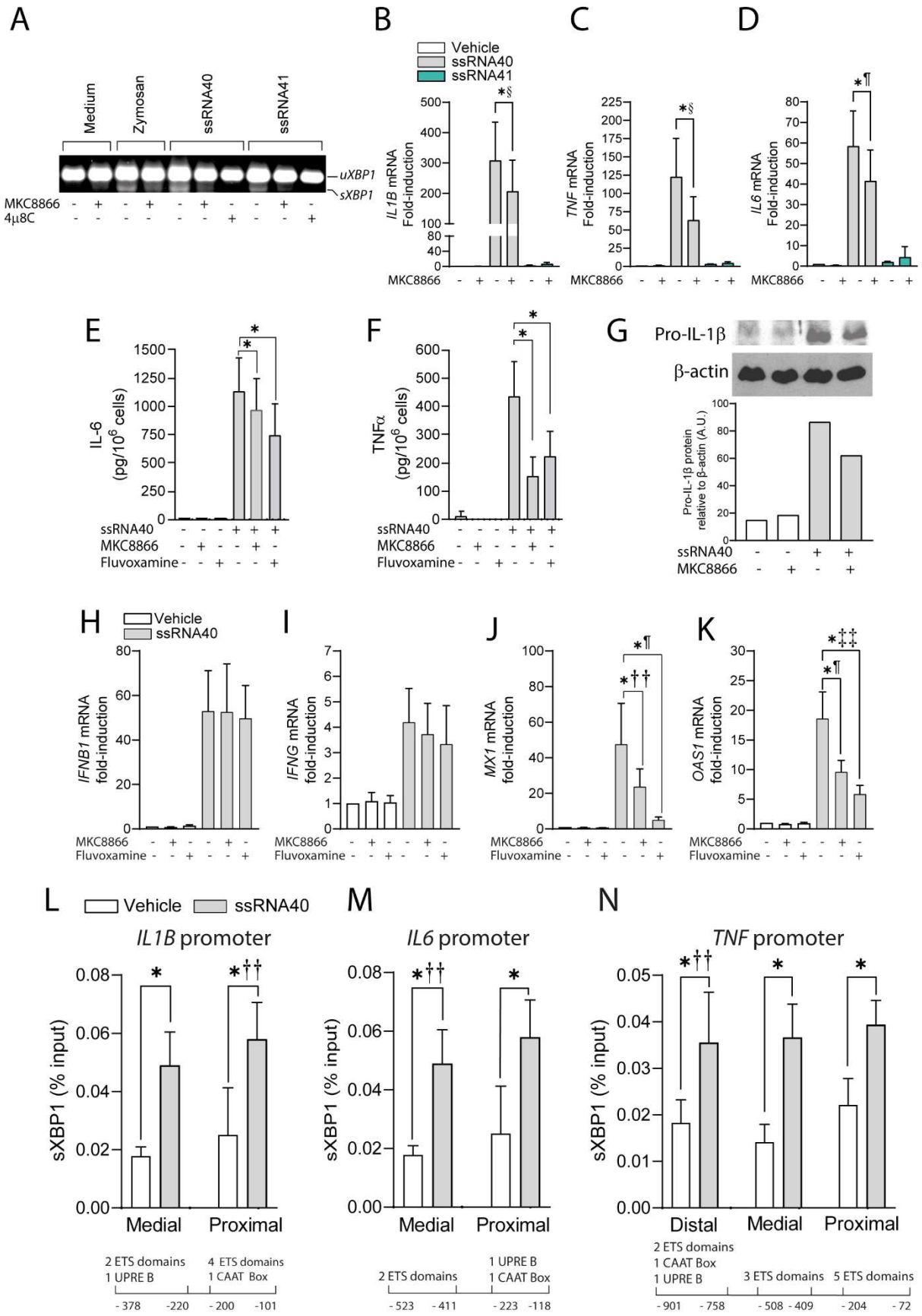

Fig 7. Effect of the TLR8 agonist ssRNA40 on MDDCs. (A) Effect of ssRNA40 and IRE1α RNase inhibitors on *sXBP1*. The RNA was collected after one hour of incubation with 10 μM MKC8866 or 20 μM 4μ8C and one hour of stimulation with 2 μg/ml of either ssRNA40 or ssRNA41 and used for the assay of *uXBP1* and *sXBP1*. (B-D) Effect of 10 μM MKC8866 on the mRNA expression of *IL1B*, *TNF*, and *IL6* mRNA. MDDCs were maintained for one hour in the presence of MKC8866 and then stimulated with ssRNA40 or ssRNA41 for 4 hours, prior to the extraction of the RNA for cytokine assays. Data are presented as mean ± SEM. *p < 0.05, **p < 0.01. §Wilcoxon matched pairs signed rank test. ¶Paired *t* test two-ways. (E and F) Effect of MKC8866 on the expression of IL-6 and TNFα protein. MDDCs were preincubated with MKC8866 for one hour and then stimulated overnight with ssRNA40. At the end of this period, supernatants were collected for cytokine ELISA assay. Data are presented as mean ± SEM. *p < 0.05. (G) Induction of the expression of pro-IL-1β by ssRNA40 and effect of MKC8866. MDDCs were treated as in the ELISA assays and after overnight incubation, cell extracts were collected and used for the assay of pro-IL-1β and β-actin proteins by Western blot. β-actin was used for normalization. A.U., arbitrary units. (H-K) Effect of MKC8866 and fluvoxamine on the expression of the mRNA encoding *IFNB1*, *IFNG*, *MX1* and *OAS1*. MDDCs were preincubated with 10 μM MKC8866 and 20 μM fluvoxamine for one hour and then stimulated with 2 μg/ml ssRNA40 for 4 hours. At the end of this time, the RNA was extracted for mRNA assay. Data are presented as mean ± SEM. *p < 0.05. ††Ratio paired *t* test. ¶Paired *t* test two-ways. ‡‡Mann Whitney test. (L-N) Effect of ssRNA40 on the binding of sXBP1 to the promoters of *IL1B*, *IL6*, and *TNF*. The captions below the graphs indicate the distance from transcription start to the nucleotide positions where PCR primers were selected. The defined sXBP1 binding sites included in the regions spanned by the primers are indicated. Samples were obtained after one hour stimulation by 2 μg/ml ssRNA40. Data are presented as mean ± SEM. *p < 0.05.††Ratio paired *t* test.